



ARTICLE

A Study of the Structural Evolution and Strength Damage Mechanisms of Pisha-Sandstone Cement Soil Modified with Fly Ash

Jian Yang, Xiaoli Li*, Hui Wang and Kaiqiang Geng

College of Water Conservancy and Civil Engineering, Inner Mongolia Agricultural University, Hohhot, 010018, China

*Corresponding Author: Xiaoli Li. Email: sjylxl@imau.edu.cn

Received: 27 December 2020 Accepted: 15 March 2021

ABSTRACT

In the present study, in order to investigate the effects of fly ash on the structural evolution and strength damage mechanism of Pisha-sandstone cement soil, unconfined compressive strength tests of Pisha-sandstone cement soil with different fly ash content levels and various ages were carried out. The apparent morphology, microstructures, and chemical compositions of the samples were observed and analyzed using ultra-depth three-dimensional microscopy, scanning electron microscopy, and XRD methods. The results revealed that the unconfined compressive strength levels of Pisha-sandstone cement soil samples displayed increasing trends with the increases in fly ash content and age. For example, when the fly ash content levels were increased from 12% to 15%, the strength of Pisha-sandstone cement soil had only slightly increased under the curing ages of 7, 28, and 60 days. In addition, the unconfined compressive strength levels of the samples with 15% fly ash content only increased 0.02%, 0.51%, and 0.54%, respectively, when compared with the samples containing 12% fly ash. It was observed that with the increases in the fly ash content, the number of pores on the outer surfaces of the samples were significantly reduced. Also, the height differences of cross-sectional gullies were reduced, and the apparent morphology was observed to be flatter. Since cement hydration creates a strong alkaline environment for reaction systems, the active degrees of the pozzolanic reactions of the fly ash were stimulated in this study. Moreover, a significant amount of the C-S-H gel phase and the stable five-membered ring structure of the mordenite and ettringite were generated, which connected the loose Pisha-sandstone particles to form a skeleton. The internal microstructures were then observed to be denser and more uniform. At the same time, the micro-pores were filled and refined by the unreacted micro-bead fly ash. Consequently, the defects in the internal microstructures were improved. Also, based on the Weibull distribution, a damage evolution model of the Pisha-sandstone cement soil was established. The analysis results of the damage variable D values during the initial damage stage, damage evolution stage, and residual damage stage of the damage process showed that the damage variables during all three stages displayed decreasing trends with the increases in the fly ash content levels and age. Therefore, based on this study's findings, it was considered that the incorporation of fly ash could effectively improve the damage degrees of Pisha-sandstone cement soil under external force conditions.

KEYWORDS

Pisha-sandstone; fly ash; strength performance; microstructure; damage variable; damage evolution model



1 Introduction

Pisha-sandstone is widely enriched in the Ordos hills of Northwestern China [1]. Pisha-sandstone has the characteristics of low degrees of diagenesis and loose structures, which result in its poor resistance to erosion. It tends to crumble into mud when exposed to water and becomes seriously eroded when exposed to wind [2]. Over time, if exposed to rainwater and wind erosion, the structural stability and strength performance of Pisha-sandstone soil will decrease, causing hidden engineering safety hazards [3]. The Erdos region economy has undergone continuous development in recent years. It has been observed that with the various construction activities for public transportation, housing, commercial development, and other sites, the Pisha-sandstone soil material in the region has been exposed to the elements. These activities have become important sources of local soil erosion.

At the same time, due to the abundant coal resources and distribution of many thermal power plants in the area, the amounts of industrial fly ash were enriched. Consequently, since fly ash has the advantages of refining pore sizes, lubricating balls, and strong pozzolanic reactions [4–6], it has not only been used to improve the working abilities of cement hydration systems, but is also conducive to improving the densities of hardened cement soil [7,8]. Fly ash has been widely used as a modifier [9–13]. For example, for the different textures of clay soil, powdered soil, and so on, a variety of cement soil have been developed which include fly ash modifications. Dong et al. [14] studied the stabilization of silty soils with different content levels of high calcium fly ash and cement, and concluded that the best stabilized effects were achieved with a 15 to 20% fly ash content. Yoobanpot et al. [15] concluded that modified cement soil formed by cement and fly ash could be effectively used to stabilize dredged sediment, and were more economical than concrete when applied to highway pavement material, with significantly increases in strength performances observed. In recent years, fly ash has been used as a modifier with cement and Pisha-sandstone bulk particles to develop Pisha-sandstone composite new materials. Such materials have been applied to road pavement bases, roadbed enclosures, farmland linings, and other engineering fields [16]. Therefore, Pisha-sandstone now has important engineering practical significance for reducing local soil erosion and achieving effective use of resources.

However, the majority of civil engineering materials have been found to experience initial damages during load-bearing processes. Since the accumulations of initial internal damages will gradually deteriorate the performance levels of a material, the load-bearing capacities of structures gradually decrease over time. These reductions in load-bearing capacities tend to affect the reliability of the material structures. As a whole multi-phase, dispersed curing material, the internal organization of cement soil contains cement stone which has been set and hardened by the hydration reactions of cementitious materials. In addition, the macroscopic organization is composed of soil particles of different shapes and sizes, and various capillary void structures formed during the preparation of the cement soil. Therefore, original damages (voids) also exist in cement soil material. At the present time, the damage degrees of geotechnical cementitious composites and asphalt mixtures have been studied in depth [17–19]. Damage evolution models are able to accurately reflect the deterioration characteristics of each material by establishing their damage evolution processes. Qu et al. [20] and Li et al. [21] established a damage evolution equation for the freeze-thaw processes of sandstone undergoing loads in acidic environments. The reliability of the models under uniaxial stress conditions were verified, which provided a theoretical basis for preventing freezing damages to rock in cold regions. Also, He et al. [22] examined the damage behaviors of cementitious materials under uniaxial stress state conditions, and simulated damage evolution processes using a continuous damage mechanics theory in order to accurately reflect the degradation characteristics of the material. In another related study, Wu et al. [23] developed a coupled thermo-mechanical damage model for the purpose of describing the mechanical responses and damage degrees of cemented coal gangue-fly ash backfill under uniaxial compression conditions, which contributed to better designing and preparation processes for stable and durable cemented coal

gangue-fly ash backfill structures. Zhang et al. [24] introduced the influencing effects of loading frequencies into the classical Chaboche damage evolution model in order to construct a new damage evolution model. The improved model was able to not only reflect the basic laws of the damage evolution and accumulation for asphalt mixtures, but also reflected the influencing effects of loading frequencies on fatigue life of the mixtures. However, there have been only a very few studies conducted regarding the damage evolution laws of modified cement soil materials and the current modeling research regarding damage predictions of cement soil materials modified with fly ash are insufficient.

In the present study, based on the above-mentioned research to date, locally enriched fly ash was utilized as a modifier, and Pisha-sandstone bulk particles were adopted as the main raw material, in order to develop Pisha-sandstone cement soil modified with fly ash. The microfabrication characteristics of the evolution of the apparent morphology, microstructures, and chemical compositions of hydrated samples of Pisha-sandstone cement soil modified with fly ash were analyzed. Then, combined with the stress-strain relationship curves of the macroscopic mechanical properties, a damage evolution model was established for the purpose of illustrating the influencing effects of fine-scale damages and the evolutionary development of the cement soil on the macroscopic mechanical properties of the material. In addition, the effects of the influence mechanism of the fly ash on the damage degrees of the Pisha-sandstone cement soil material were explained from the perspective of damage mechanics. The results obtained in this study which provided a theoretical basis for the future applications of Pisha-sandstone cement soil modified with fly ash in practical engineering projects.

2 Materials and Experiments

2.1 Raw Material

The red Pisha-sandstone soil samples used in this study's experiments were obtained from the Zhungeer Banner of Ordos City in Inner Mongolia, as shown in Fig. 1. The physical parameters of the Pisha-sandstone samples are shown in Tab. 1. The percentage content level of the red Pisha-sandstone particle size $d < 0.25$ mm was 93.06%. The percentage content level of $0.25 \text{ mm} \leq d < 0.5$ mm was 3.5%, and the percentage content level of $d \geq 0.5$ mm was 3.44%. Therefore, the red Pisha-sandstone was considered to be a fine sand. The Pisha-sandstone samples were first ground and crushed. Then, following a natural air-drying process, the samples were filtered through a 2.36 mm sieve for future use. The cement utilized in this study was Jidong P-O42.5 ordinary Portland cement with a fineness of 6.3%, and a density of $3.14 \times 10^3 \text{ kg/m}^3$. The volume stability was qualified, and the 28-day compressive strength was 48.7 MPa. The fly ash was taken from first grade fly ash of the Jinqiao Thermal Power Plant in Hohhot, and the main chemical components are shown in Tab. 2. The water used in this study's experimental tests was ordinary tap water. The XRD phase analysis results of the Pisha-sandstone and fly ash are detailed in Fig. 2.

2.2 Specimen Preparation

In accordance with the "Test Regulations for Stabilized Materials of Inorganic Bonds in Highway Engineering" (JTJ E51-2009), in order to explore the influencing effects of the fly ash on the structural evolution and strength damage mechanism of the Pisha-sandstone cement soil, a $\text{Ø}50 \times H50$ specimen was produced. In addition, five groups of fly ash content were designed at 0%, 6%, 9%, 12%, and 15%, respectively. The cement content was set at 10%, and three parallel specimens were made for each group. The mixture formulation design of the materials is shown in Tab. 3. Prior to constructing the specimen, a water content of 80% was first added to the Pisha-sandstone and mixed well. The Pisha-sandstone soil was sealed in a bag and left undisturbed for a minimum of 24 h. The cementitious material and 20% of the water were added to the Pisha-sandstone and mixed well, and then directly installed in a mold and compacted. After demolding, the specimen was placed into a standard curing box with a humidity of 95% and a temperature of $(20 \pm 2)^\circ\text{C}$ for periods of 7, 28, and 60 days. After reaching the curing age, in

accordance with the “Standard for Soil Test Method” (GB/T 50123-2019), the specimen was soaked in water at a temperature of $20 \pm 2^\circ\text{C}$ for 24 h. Unconfined compressive strength tests were carried out after water saturation was complete. The preparation process is shown in Fig. 3.

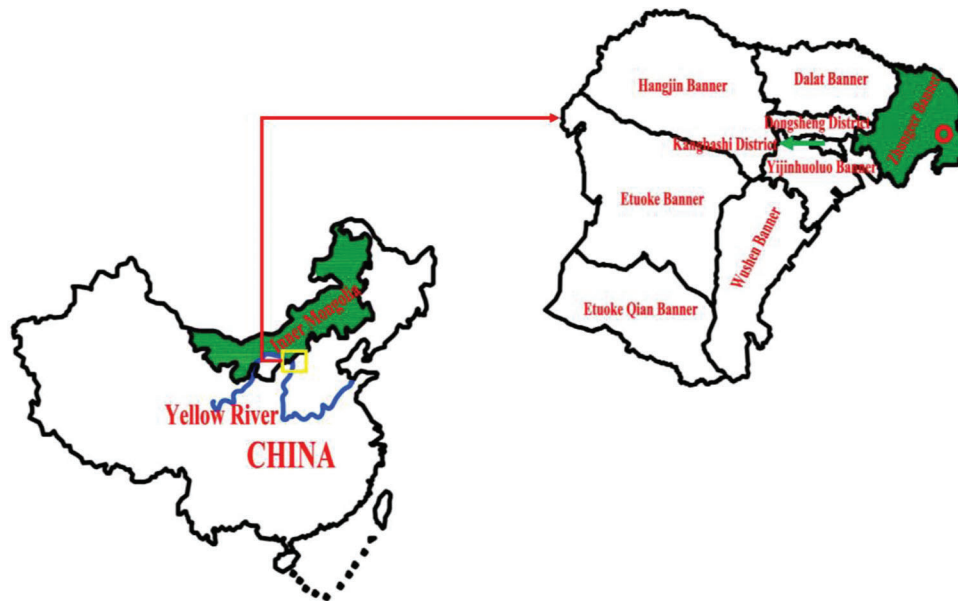


Figure 1: This is the location of Pisha-sandstone

Table 1: Basic physical indicators of red Pisha-Sandstone

Saturated water content (%)	Liquid limit (%)	Plastic limit (%)	Plasticity Index	Permeability coefficient (mm s^{-1})	Porosity (%)	Density (g cm^{-3})	Classification of soil
18.60 ~ 19.50	29.30	19.60	9.00	5.20×10^{-3}	31.04 ~ 35.15	1.85 ~ 1.96	sandy soil

Table 2: Main chemical compositions and physical properties of materials/%

Material	SiO_2	Al_2O_3	CaO	Fe_2O_3	MgO	other	Loss of ignition
Cement	21.29	5.20	63.50	4.11	0.49	5.50	3.1
Fly ash	59.27	25.35	6.11	6.43	0.76	4.08	≤ 5
Pisha-sandstone	72.00	11.00	5.00	3.00	1.00	8.00	—

2.3 Test Method

2.3.1 Unconfined Compressive Strength Test

The specimens were cured to the specified ages in a standard curing box. Then, the test specimens were removed and a WDW-50 universal testing machine was utilized for this study’s unconfined compressive strength tests. The maximum load was 50 kN and the shear rate was 2 mm/min.

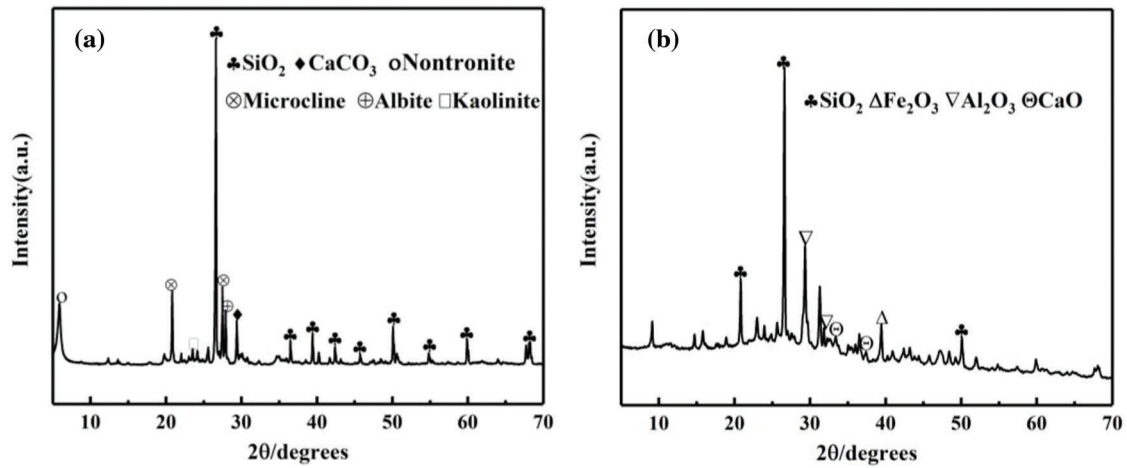


Figure 2: XRD analyses of Pisha-sandstone and fly ash (a) XRD of Pisha-sandstone (b) XRD image of fly ash

Table 3: Mixture formulation design of materials used for tests

Symbol	Specimen volume (cm ³)	Standard quality (g)	Pisha-sandstone (g)	Cement (g)	Fly ash (g)	Total water consumption (g)	Soaking water (g)	Reserved water (g)
FA-0	98.125	203.07	165.97	18.44	0	16.82	13.46	3.36
FA-6	98.125	203.07	154.91	18.44	11.07	17.10	13.68	3.42
FA-9	98.125	203.07	149.37	18.44	16.60	17.24	13.79	3.45
FA-12	98.125	203.07	143.84	18.44	22.13	17.38	13.90	3.48
FA-15	98.125	203.07	138.31	18.44	27.66	17.51	14.01	3.50

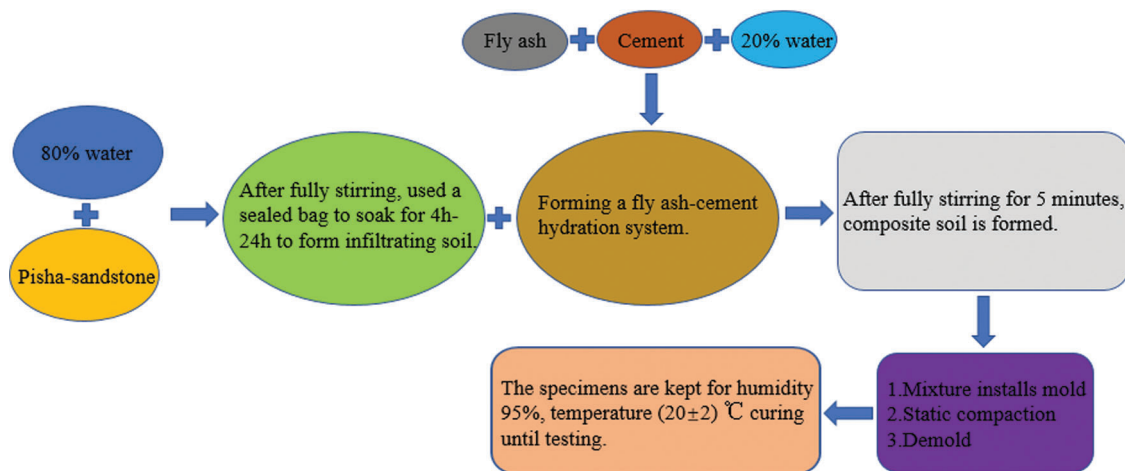


Figure 3: Specimen preparation process

2.3.2 pH Value Determination

The specimens which had completed the unconfined compressive strength tests were evenly divided into approximately four parts by height, and 0.25 g samples were taken from each part. Then, the 10 g samples

were rolled into powder and placed into test tubes in order to achieve a soil-water ratio of 1:5 sample solution. Then, after being allowed to stand undisturbed for 24 h, the supernatant was removed from the test tubes in order to determine the pH values.

2.3.3 Three-Dimensional Microscopy of Ultra-Deep Field Test

After reaching the specified curing age of 28 days, the specimens were removed from the standard curing box and the moisture on the surfaces of the specimens was repeatedly absorbed with filter paper. The surfaces of the specimens were then gently dusted with a brush in order to remove any material which had fallen off the surfaces. Finally, the specimens were placed on a load table. An ultra-depth three-dimensional microscope (type Z16APOA) from Leica, Germany was used to observe the upper and lower external surfaces of the cylindrical specimens with fly ash content levels of 0%, 6%, 12%, and 15%, respectively. Then, after ingesting and integrating apparently accurate 3D images of the specimens, Leica Map software was used for this study's contour extractions and 3D stereoscopic image constructions of the ingested and integrated 3D map at 50x magnification.

2.3.4 SEM and XRD Test

The test samples were split prior to the SEM tests. Then, the test parts were treated using gold spraying and vacuum sublimation methods. The microstructures of the Pisha-sandstone cement soil modified with fly ash were observed using a COXEM EM-30AX Plus high-resolution tabletop scanning electron microscope. The changes in chemical composition of the samples were analyzed using a Rigaku smartlab9k X-ray diffractometer.

3 Experimental Results

3.1 Effects of the Fly Ash on the Unconfined Compressive Strength and pH Values of the Pisha-sandstone Cement Soil

Fig. 4 shows the variations in the unconfined compressive strength levels and the pH levels of the Pisha-sandstone cement with different fly ash content and at different ages. As shown in Fig. 4a, at each curing age, when the fly ash content was gradually increased from 0% to 12%, the strength levels had increased significantly. However, when the fly ash content increased from 12% to 15%, the strength levels of the Pisha-sandstone cement soil had only slightly increased. In particular, at the curing age of 7 days, the compressive strength when the fly ash content is 15% was only observed to increase by 0.02%, when compared with the compressive strength when the fly ash content was 12%. It was also found that the increases were 0.51% and 0.54% at 28 days and 60 days of age, respectively. These results indicated that the early fly ash glass network formation anions ($[\text{SiO}_4]^{4-}$, $[\text{AlO}_4]^{5-}$) were denser and more stable [4,25], and the pozzolanic reaction activities were relatively weak. In addition, it was observed that when the amount of fly ash content reached a certain value and increases in the content levels continued, the strength level increases were limited.

This study found that the compressive strength levels of the Pisha-sandstone cement soil increased rapidly with the increases in age when the amount of fly ash content remained unchanged. In particular, the rates of strength formation were extremely significant when the curing age reached 28 days, with the compressive strength levels becoming increased by 73.74%, 85.12%, 64.13%, 56.20%, and 56.97%, respectively, when compared with that of the 7-day curing age. Furthermore, the compressive strength levels at 60 days of curing were increased by 57.30%, 73.41%, 50.10%, 45.54%, and 45.82%, respectively, when compared with that of the 7-day curing age. Therefore, it was indicated that as the curing time increased, the active substances in the fly ash had participated more fully in the cement hydration reactions and the secondary reactions were more active. It was found that increased calcium hydrated silicate (C-S-H) gel phase and calcium alumina (AFt) were generated, forming a network-like structure within the specimen which connected the Pisha-sandstone particles to form a skeleton. Therefore, the strength of the cement soil had been effectively enhanced and the strength damage deterioration rates had been hindered.

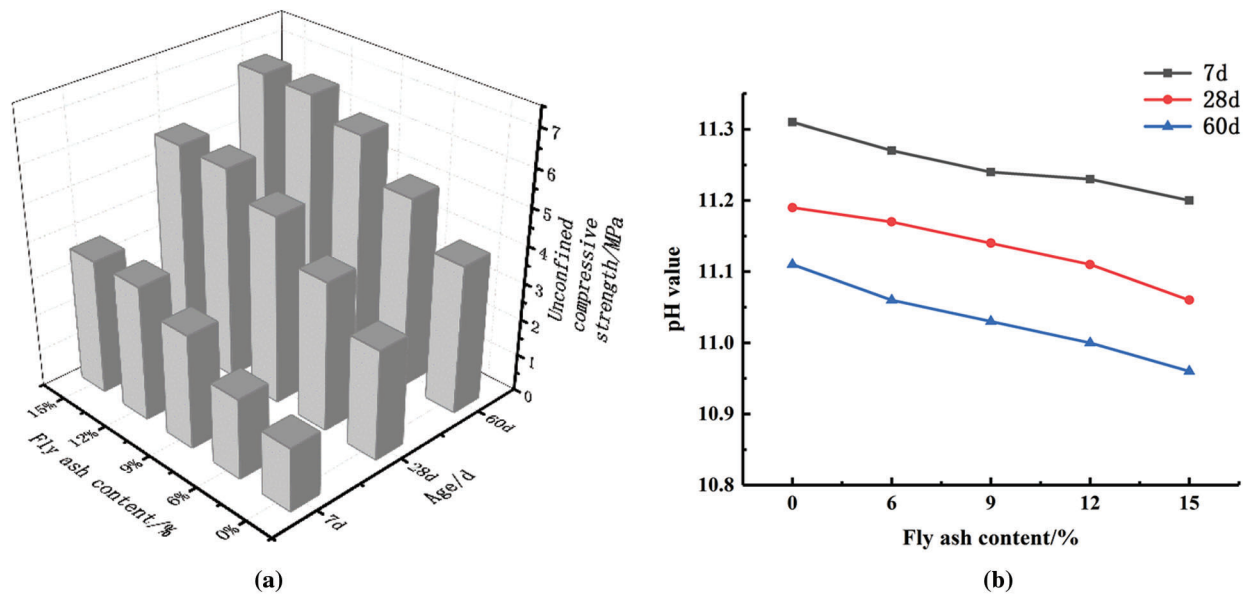


Figure 4: Unconfined compressive strength and pH value of cement soil under different fly ash content and age (a) Unconfined compressive strength (b) pH value

As can be seen in the analysis results shown in Fig. 4b, the pH values of the Pisha-sandstone cement soil which had been modified with fly ash displayed a slight downward trend with the increases in the fly ash content levels and curing age. This is due to the fact that, with the addition of the fly ash, the active substances in the fly ash had reacted materially with the CH produced by the hydration of cement. Meanwhile, the hydration reactions released large amounts of hydration heat, which stimulated the reaction speeds of the material. As a result, the OH⁻ in the hydration system was gradually consumed, which caused decreases in the pH values of the system. It was also further indicated that the hydration reactions had slowly continued with the increases in the fly ash content levels and age. Since hydration systems in strong alkaline environments tend to generate gel substances which have positive effects on the formation of the compressive strength of a specimen, this was considered to be the main cause of the resistance to the strength damage processes.

3.2 Effects of the Addition of Fly Ash on the Apparent Structure of the Pisha-Sandstone Cement Soil

The surface morphological characteristics of Pisha-sandstone cement soil modified with fly ash were observed using an ultra-deep-field three-dimensional microscope (type Z16APOA) from Leica (Germany). Then, the evolution mechanisms of the apparent structures of the Pisha-sandstone cement composite soil with different fly ash content levels were analyzed. As shown in Fig. 5, the apparent pores of the samples with 0% fly ash content were interconnected to form ravines, and the apparent average height difference was 232 μm . Also, it was observed that, with the increases in the fly ash content, the evolution rates of the interpenetration of the ravines had slowed down, with the appearance becoming gradually uniform and dense. The average height differences of the samples with 6%, 12%, and 15% fly ash content were 199 μm , 145 μm , and 127 μm , respectively, which were decreases of 33 μm , 87 μm , and 105 μm when compared with the average height differences of the samples with 0% fly ash content, respectively. It can also be seen in the figure that with the increases in fly ash content, the apparent morphology of the Pisha-sandstone cement soil undulation had decreased, and the surfaces tended to be flat.

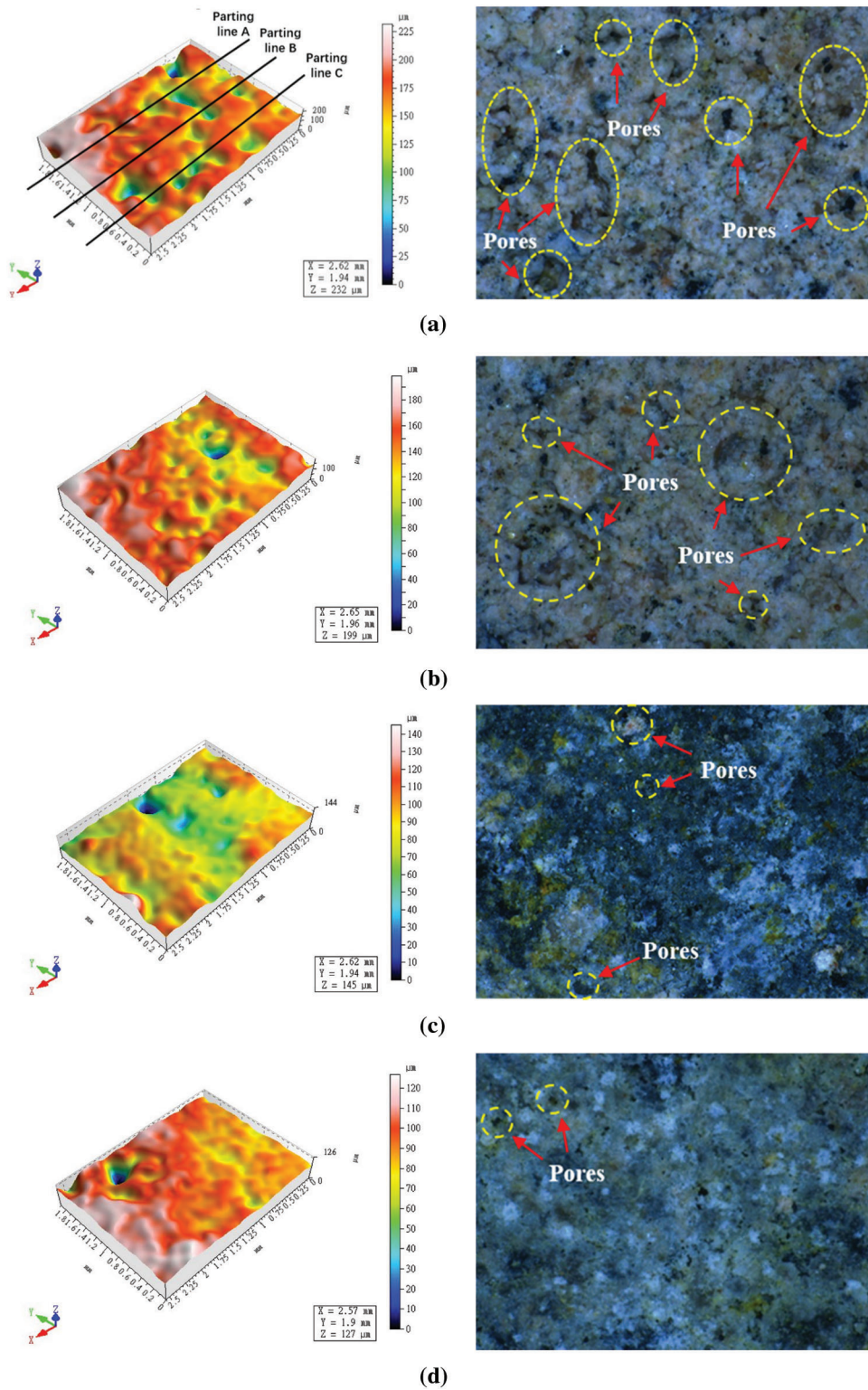


Figure 5: 3D map of super depth of field of Pisha-sandstone cement soil modified with fly ash (a) FA-0 (b) FA-6 (c) FA-12 (d) FA-15

In order to more accurately compare the evolution of the apparent morphology and the micro-pores with different fly ash content levels, the apparent 3D map under different fly ash content conditions was cut horizontally into four equal parts using Leica Map software. The interface height difference changes of the three-section with fly ash content levels of 0%, 6%, 12%, and 15% were analyzed, as detailed in Fig. 6. The adopted 3D graph cutting method is shown in Fig. 5a. As can be seen from the analysis results of the cut section graph, the vertical positions of the three sections of the apparent depth-of-field 3D images of the specimens with 15%, 12%, and 6% fly ash content levels were shifted upward when compared with those with 0% fly ash content. The maximum height differences of the longitudinal holes at Sections A, B, and C had moved up 81.2 μm , 80.1 μm , 40.2 μm , 82.6 μm , 77.3 μm , 60.4 μm , 205.3 μm , 132.3 μm , and 105.4 μm , respectively. At the same time, this study's comparison with the original samples at different observation locations on the specimen surfaces revealed that with the increases in fly ash content, the specimen surfaces were flatter than those of the unadulterated samples. These findings indicated that as the fly ash content levels became higher, the active SiO_2 in it had contributed to the hydration of the cement causing more gel phase to be produced. The surfaces and structures of the loose Pisha-sandstone particles were wrapped and cemented while the pores became filled with unreacted micro-bead fly ash. This had resulted in the composite fly ash and Pisha-sandstone cement soil becoming more compact.

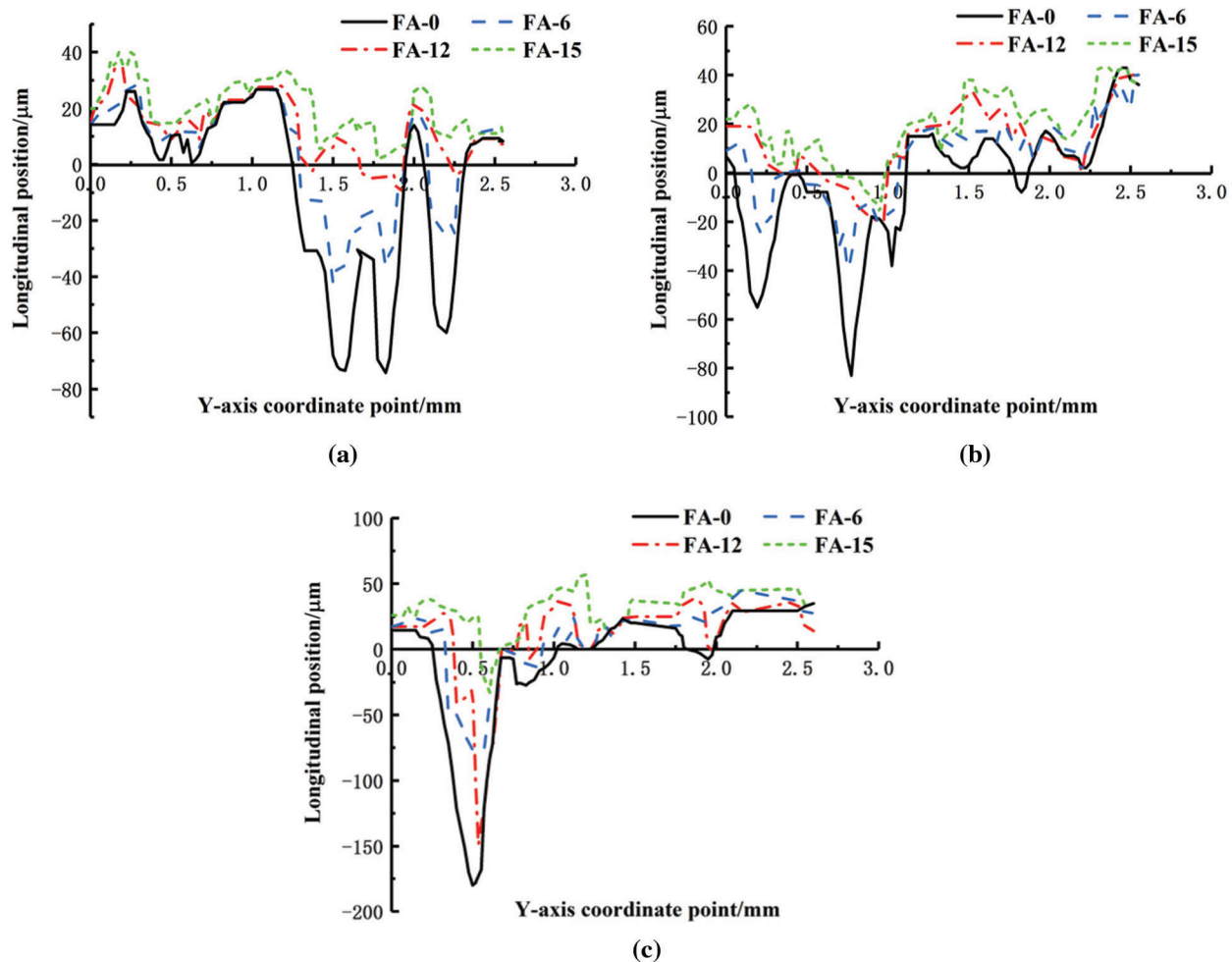
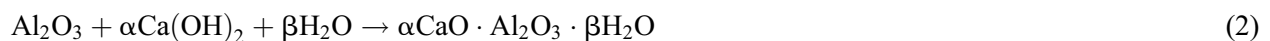


Figure 6: Cutaway diagram of samples with different fly ash content (a) Parting line A (b) Parting line B (c) Parting line C

3.3 Effects of the Addition of Fly Ash on the Microstructures of the Pisha-Sandstone Cement Soil

The incorporation of fly ash is known to be beneficial in improving the height differences of the gullies in the apparent cross-sections of Pisha-sandstone cement soil and reducing the number of holes. In the present study, in order to further analyze the effect mechanisms of the fly ash content levels on the microstructures of the Pisha-sandstone cement soil, Pisha-sandstone cement soil specimens with a curing age of 28 days and fly ash content levels of 0%, 6%, 12%, and 15%, respectively, were selected for microstructural observations under 2,000x magnification.

Fig. 7 shows the scanning electron microscopy images of the examined Pisha-sandstone cement soil specimens with different fly ash content levels. It can be seen in the Figs. 7a and 7b, the specimens appeared to display micro-cracking and porosity in the cement matrix. In particular, the micro-porosity and fine cracks of the unblended fly ash cement soil specimens were significantly larger than those with 6% fly ash content. Moreover, only sporadic flocculent and needle-like calcium silicate hydrate (C-S-H) gel phases were observed to be scattered on the surfaces of the Pisha-sandstone particles. Also, small amounts of rod-shaped ettringite (AFt) crystals existed in the form of clusters, which formed strong bonds between the Pisha-sandstone particles, resulting in the overall structures being relatively dense. As can be seen in Figs. 7c and 7d, with the increases in fly ash content, large numbers of needle-like and flocculent calcium silicate hydrate (C-S-H) gel phases, characterized with intricate growth and dense textures, were attached to the surfaces of the cement matrix, and had penetrated into the pores to form dense textured network structures. The ettringite (AFt) crystals were observed to often be interspersed in the fine pores and attached to the surface layers of the cement soil matrix in the forms of miscellaneous interweaving and overlapping clusters, which improved the integrity and stability of the hydration material, and potentially played a role in cementing connections. At the same time, it can be clearly seen in Fig. 7c that the incompletely reacted ball-shaped fly ash particles had physically filled and refined the micropores between the calcium silicate hydrate (C-S-H) gel particles. Due to the fact that the fly ash had a high content of glassy phase, it was found that after adding fly ash into the cement hydration system, the active SiO_2 anions in the glass networks had higher degrees of depolymerization, which had the ability to quickly react with the $\text{Ca}(\text{OH})_2$ in the system. Consequently, the pozzolanic reaction process was accelerated and the fly ash-cement hydration system became more active. Then, large amounts of calcium silicate hydrated (C-S-H) gel and ettringite (AFt) were generated, which were adsorbed and cemented on the surfaces of the Pisha-sandstone particles and connected to form a complex skeleton between the particles. This caused the inside areas of the Pisha-sandstone cement soil to become more uniform and compacted. Also, due to the small size effects and spherical shape effects of the fly ash [5], the internal pore structures of the Pisha-sandstone cement soil were filled, improved, and refined. Therefore, it was considered in this study that the addition of fly ash had promoted the continuous enhancement of the strength properties of the Pisha-sandstone cement soil. The pozzolanic reaction process can be expressed by the following [15,26]:



3.4 XRD Analysis of the Pisha-Sandstone Cement Soil Samples Modified by Fly Ash Hydration

Fig. 8a illustrates the XRD patterns of 28-day hydration samples of Pisha-sandstone cement soil with different fly ash content levels (2θ is 5° to 70°). It can be seen in the figure that there were no significant differences observed during the basic phases of the Pisha-sandstone cement soil with different fly ash content. The main phases of each specimen contained ettringite (AFt), calcium hydroxide (CH), calcite (CaCO_3), quartz (SiO_2), nontronite, and Albite. Also, a new phase of mordenite was formed when the fly ash content was 15%. Fig. 8b shows the XRD patterns of the hydration samples with various fly ash

content levels after enlarging at 5° to 19° . As detailed in the figure, when comparing the characteristic diffraction peaks of the CH ($2\theta \approx 18.0^\circ$) and AFt ($2\theta \approx 9.2^\circ$) in the samples with various fly ash content, it was found that with the increases in the fly ash content, the intensities of the characteristic diffraction peaks of the CH of the specimens gradually weakened. Meanwhile, the characteristic diffraction peaks of the AFt were observed to gradually increase. This was determined to be due to the fact that with the incorporation of fly ash, the fly ash had reacted materially with the CH to stimulate the activities of the pozzolanic reactions, thereby generating large amounts of ettringite (AFt) and reducing the amount of CH. At the same time, since the mordenite crystal structures had large numbers of five-membered rings which facilitated energy stabilization [27–30], structurally stable skeletons had been formed between the Pisha-sandstone particles.

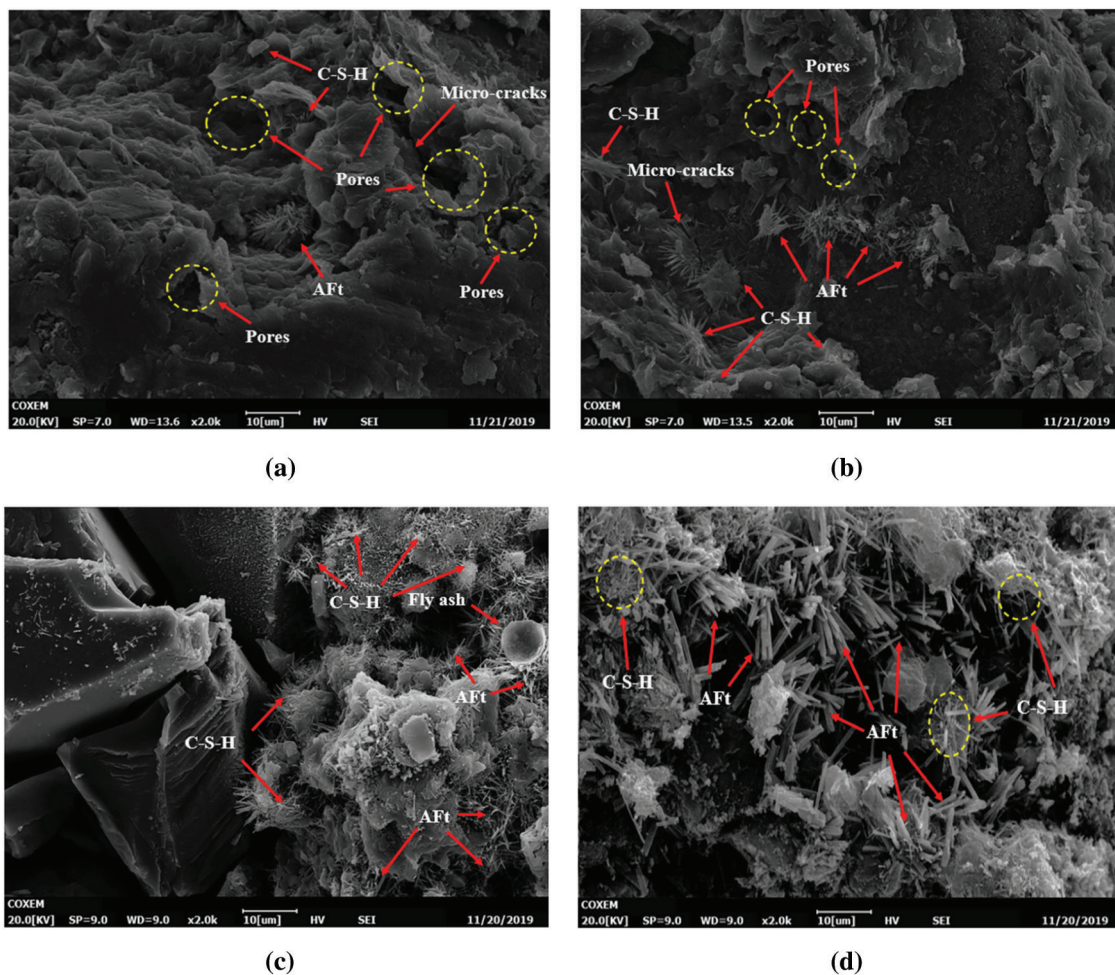


Figure 7: The microstructure diagram of each sample magnified 2,000x (a) FA-0 (b) FA-6 (c) FA-12 (d) FA-15

3.5 Damage Evolution Law of the Pisha-Sandstone Cement Soil Modified with Fly Ash Based on the Weibull Distributions

Due to the large number of pores between the hydrated gel and the Pisha-sandstone particles within the cement soil material [31], it was found that under the actions of external loads, the cement soil material gradually showed a tendency of deterioration. In other words, damages occurred [32,33]. Therefore,

based on the Weibull statistical distributions of the micro-element strength levels of the rock, concrete, and other stone [34–36], the Weibull distribution of two-dimensional parameters was used to describe the evolution law of the damage degrees of the Pisha-sandstone cement soil modified with fly ash [37,38].

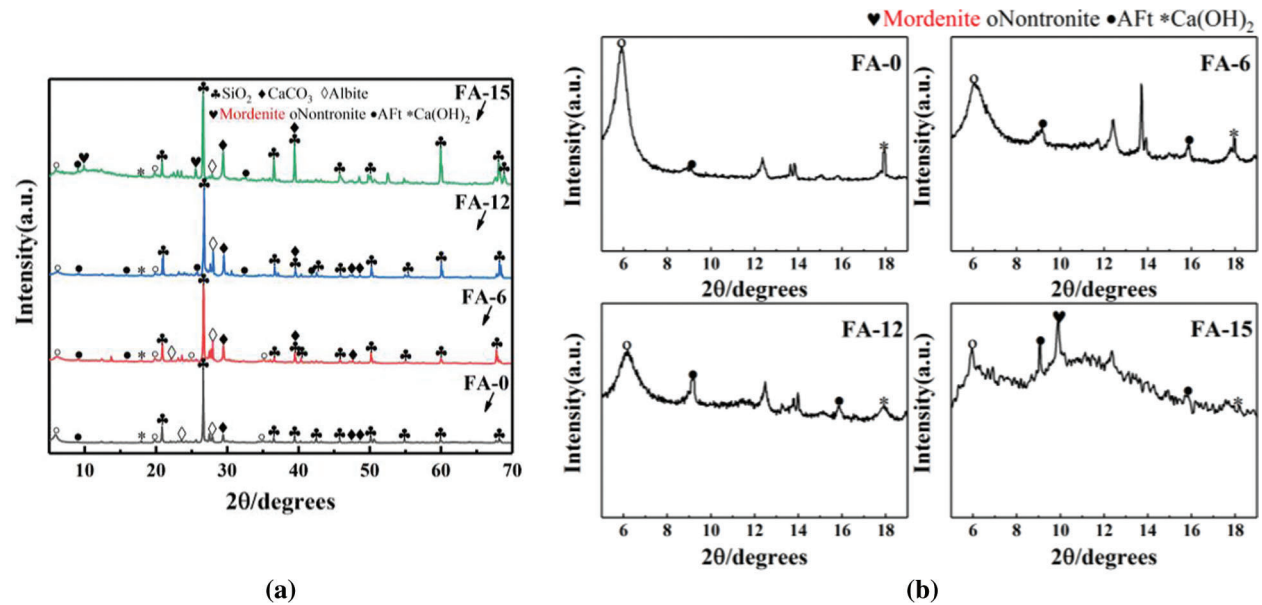


Figure 8: XRD patterns of Pisha-sandstone cement soil with different fly ash content (a) The diffraction angle is 5°~70° (b) The diffraction angle is 5°~19°

The distribution density function was given as follows:

$$P(f) = \frac{m}{F} \left(\frac{f}{F}\right)^{m-1} \exp\left[-\left(\frac{f}{F}\right)^m\right] \tag{3}$$

where f is the strength level of the micro-materials; m and F are the Weibull distribution parameter; $P(f)$ determines the damage rate of the micro-unit, and the micro-unit damage accumulation results are macro damages.

The damage degrees indicate the quantity of micro-unit defects which directly influence the micro-unit strength levels. The relationship between the damage variable D and the probability density of the micro-unit damage can be expressed as follows:

$$\frac{dD}{d\varepsilon} = P(f) \tag{4}$$

Therefore, by integrating Eq. (4), the relational expression of the damage variable D can be obtained as follows:

$$D = \int_0^f P(f)df = 1 - \exp\left[-\left(\frac{f}{F}\right)^m\right] \tag{5}$$

Lemaitre’s hypothesis for equivalent strain proposes a constitutive relationship based on statistical damages, which can be expressed as follows [39,40]:

$$[\sigma^*] = \frac{[\sigma]}{1-D} = \frac{[C][\varepsilon]}{(1-D)} \quad (6)$$

where $[C]$ represents the elastic matrix of the material; D is the damage variable; $[\sigma]$ denotes the nominal stress matrix; $[\sigma^*]$ indicates the effective stress matrix; and $[\varepsilon]$ is the strain matrix.

Therefore, based on the concept of continuous damage mechanics [41,42], the damage anthropomorphic relationship for cement soil under no lateral limit compressive strength tests can be deduced as follows:

$$\sigma = E\varepsilon(1-D) \quad (7)$$

Since the Mohr-Coulomb yield criterion reflected the strength levels of the cement soil microelements with higher accuracy [43–46], the damage guidelines for the cement soil were also based on the Mohr-Coulomb yield criterion, and its micro-unit strength was as follows:

$$f = (\sigma^*) = \sigma_1^*(1 - \sin \varphi) - \sigma_3^*(1 + \sin \varphi) = 2C \cos \varphi \quad (8)$$

where φ indicates the internal friction angle; C denotes the cohesion; $\sigma_1, \sigma_2, \sigma_3$ ($\sigma_2 = \sigma_3$) are the three principal stresses; ε_1 indicates the first principal strain; and $\sigma_1^*, \sigma_2^*, \sigma_3^*$ ($\sigma_2^* = \sigma_3^*$) are the effective stress.

Therefore, the following were derived using Hooke's Law and Eq. (6):

$$\varepsilon_1 = \frac{\sigma_1^* - 2\mu\sigma_3^*}{E} \quad (9)$$

$$\sigma_i^* = \frac{\sigma_i}{1-D} \quad (10)$$

Then, the micro-unit strength of the cement soil could be expressed as:

$$f = \frac{E\varepsilon_1[(\sigma_1 - \sigma_3) - (\sigma_1 + \sigma_3) \sin \varphi]}{\sigma_1 - 2\mu\sigma_3} \quad (11)$$

Since this study's experiments were performed under uniaxial compression conditions, the micrometric strength was expressed as follows:

$$f = E\varepsilon(1 - \sin \varphi) \quad (12)$$

Therefore, by substituting Eqs. (12) and (5) into Eq. (7), the following was obtained:

$$\sigma = E\varepsilon \exp \left\{ - \left[\frac{E\varepsilon(1 - \sin \varphi)}{F} \right]^m \right\} \quad (13)$$

$$\frac{d\sigma}{d\varepsilon} = Ee^{-\left[\frac{E\varepsilon(1 - \sin \varphi)}{F} \right]^m} \left\{ 1 - m \left[\frac{E\varepsilon(1 - \sin \varphi)}{F} \right]^{m-1} \right\} \quad (14)$$

When the strain reached the peak stress level of the uniaxial compressive stress-strain curve, the curve geometry should be satisfied $\varepsilon = \varepsilon_{max}, d\sigma/d\varepsilon = 0, \varepsilon_{max}$, which will be the value of the strain under peak load conditions.

$$F = (1 - \sin \varphi) E \varepsilon m^{\frac{1}{m}} \quad (15)$$

Then, based on Eqs. (15) and (13) and the curve geometry condition $\varepsilon = 0, d\sigma/d\varepsilon = E$, it follows that:

$$m = \frac{1}{\ln(E\varepsilon_{max}) - \ln \sigma_{max}} \tag{16}$$

Therefore, by substituting Eq. (15) into Eq. (5), the evolution equation for the soil and water damages will be as follows:

$$D = 1 - \exp\left[-\frac{1}{m} \left(\frac{\varepsilon}{\varepsilon_{max}}\right)^m\right] \tag{17}$$

The intrinsic equation for the evolution of the cement soil damages under uniaxial pressure conditions was derived from Eqs. (15) and (13) as follows:

$$\sigma = E\varepsilon \exp\left[-\frac{1}{m} \left(\frac{\varepsilon}{\varepsilon_{max}}\right)^m\right] \tag{18}$$

3.5.1 Analysis of the Damage and Deformation Characteristics of the Pisha-sandstone Cement Soil Modified with Fly Ash

According to the damage evolution Eq. (17), the value of the damage variable D could be calculated for the entire deformation damage process of the Pisha-sandstone cement soil modified with fly ash. This study selected the curing age of 28 days as an example. The relationships between the damage variables D and the stress-strain curves of the Pisha-sandstone cement soil specimens with different fly ash content levels are shown in Fig. 9. Therefore, based on the failure process of the Pisha-sandstone cement soil under uniaxial compression conditions, the damage evolution curves were roughly divided into three stages as follows:

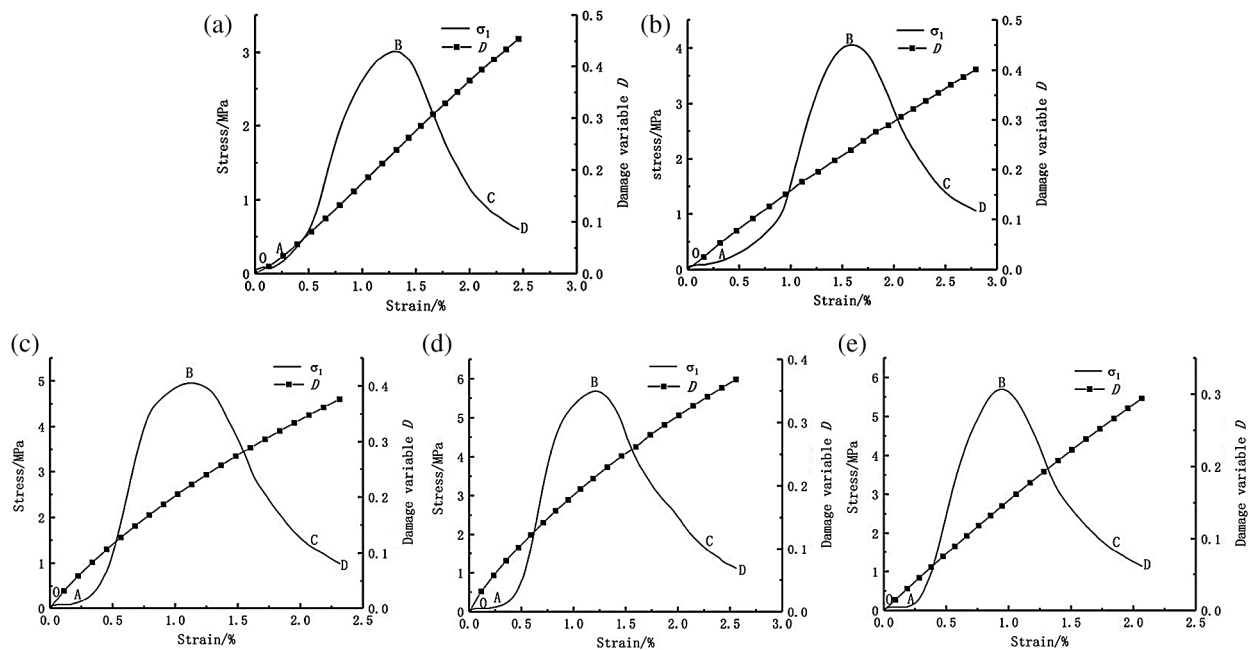


Figure 9: Damage evolution curve of Pisha-sandstone cement soil with different fly ash content (a) FA-0 (b) FA-6 (c) FA-9 (d) FA-12 (e) FA-15

1. Initial damage stage (OA section): This stage mainly refers to the compaction stage of the Pisha-sandstone cement soil. As can be seen in Fig. 9, during the compaction stage of the Pisha-sandstone cement soil, the damage variables in Fig. 9a slowly increased in the early stages of the compression deformation. Meanwhile, it can be seen that the damage values shown in Figs. 9b–9e increased rapidly during the compaction stage. Fig. 9 also illustrates that when the fly ash content was 0%, the strength levels of the specimens in the compaction stage of the Pisha-sandstone cement soil had increased significantly faster than that of the specimens with fly ash content levels of 6%, 9%, 12%, and 15%, respectively.

2. Damage evolution development stage (AC section): As shown in Fig. 9a, for the specimens from the linear elastic stage to the destruction stage, the damage variables increased significantly faster than during the compaction stage. Figs. 9b–9e show that the growth rates of the damage variables of the specimens gradually became smaller. The new cracks were generated which gradually penetrated the specimens, as shown in Figs. 10a, 10b.

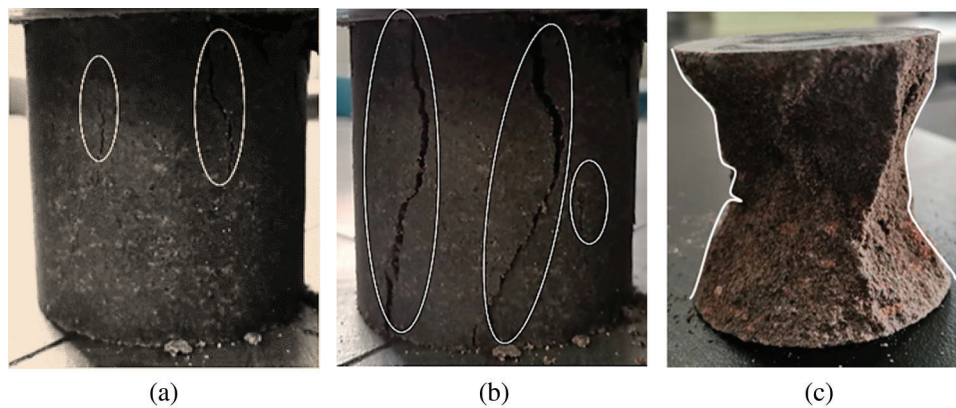


Figure 10: Diagram of damage and destruction process of test block under load (a) Microcrack generation and (b) Microcrack penetration (c) Specimen damage propagation

3. Residual damage stage (CD section): In the CD section shown in Fig. 9, it can be seen that the CD damage variable D values still grew rapidly (Fig. 9a). Meanwhile, in Figs. 9b–9e, the growth can be seen to have become progressively flatter. This was due to the fact that the specimens had been essentially destroyed by that time, and the load-bearing capacities were drastically reduced. The damage degrees of the specimens following the residual strength stage are shown in Fig. 10c.

3.5.2 Effects of the Fly Ash Content Levels and Ages on the Damage Evolution of the Pisha-Sandstone Cement Soil

The values of the damage variables D for each stage of the Pisha-sandstone cement soil were calculated in this study with different fly ash content levels and ages, as detailed in Fig. 11.

It can be seen from the analysis results shown in Fig. 11 that under uniaxial compression conditions, when the curing ages were 7, 28, and 60 days, the values of the damage variable D at each stage displayed a linear downward trend with the increases in the fly ash content. It was found that under different fly ash content levels and ages, the values of the damage variable D during the compaction stage were much smaller than the D values at the peak points and during the residual strength stage, which indicated that almost no damage had occurred during the compaction stages of the specimens.

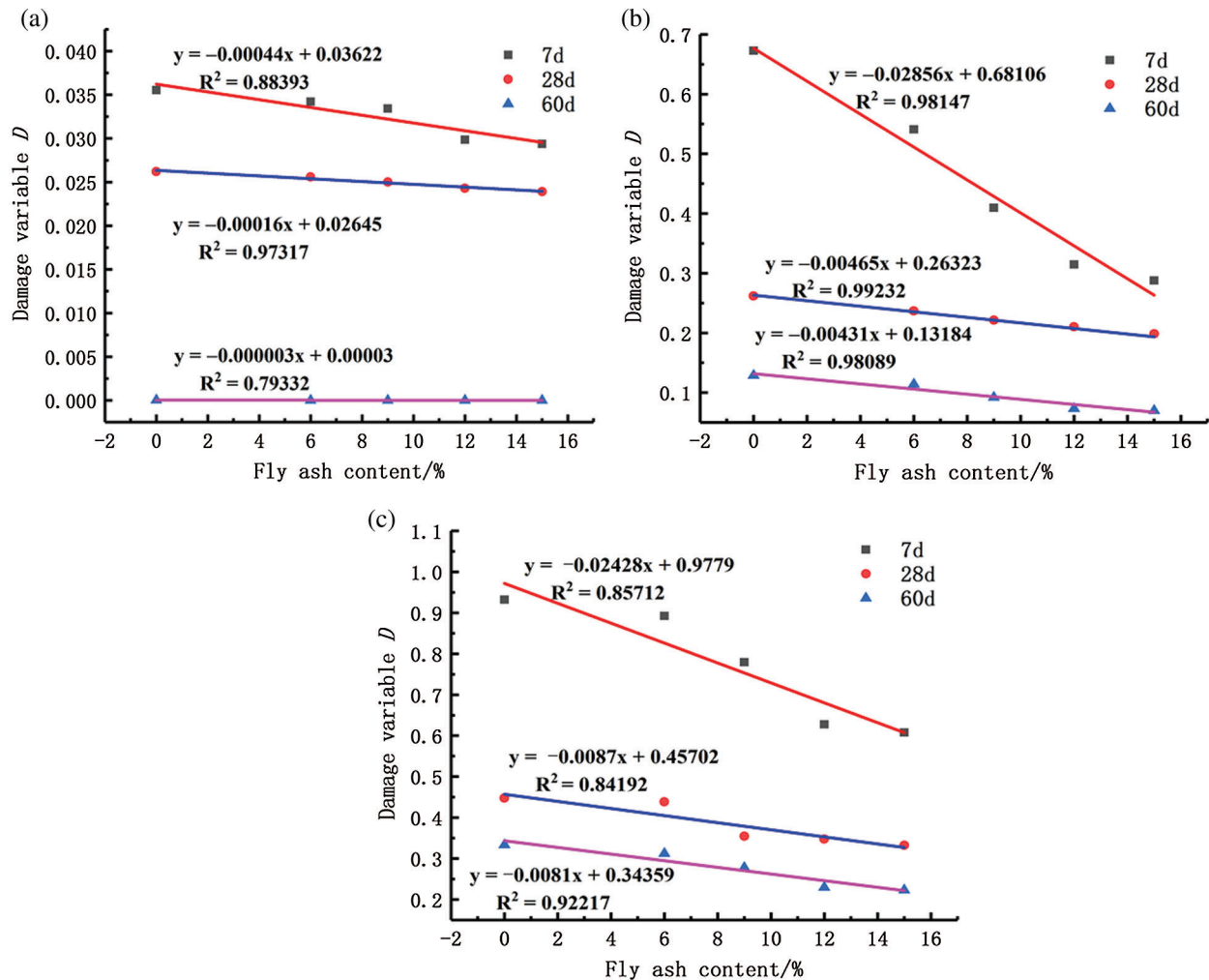


Figure 11: Variation curve of damage variable D with fly ash content and age in each stage (a) D value during compaction stage (b) D value at peak point (c) D value during Residual strength stage

The values of the damage variable D at each stage displayed decreasing trends with the increases in the curing ages, and the slopes of the fitting curves were getting smaller. Furthermore, it was found that the greater the curing age was, the values of the damage variable D of the specimens at each stage were observed to decrease more slowly with the increases in the fly ash content. At the peak points and during the residual strength stage, it was found that under the different fly ash content level conditions, the values of the damage variable D at 28 days and 60 days were similar. Meanwhile, the differences were larger compared with the 7-day curing age. This was determined to be due to the fact that when the curing age increased, the cement hydration in the Pisha-sandstone cement soil was more sufficient and accompanied by the production of large amounts of $\text{Ca}(\text{OH})_2$. The active SiO_2 and Al_2O_3 in the fly ash promoted reactions with the CH, which generated gel phases, such as calcium silicate hydrate (C-S-H). This in turn formed network structures which improved the compactness of the internal structures of the specimens, as well as increasing the cementation between the crystals. In turn, the specimens' resistance abilities to damages were improved and the deterioration rates of the internal structures of the specimens were effectively slowed down.

4 Conclusion

The results of this study confirmed that fly ash can improve the surfaces and internal structures of Pisha-sandstone cement soil. It was found that due to the incorporation of fly ash, violent pozzolanic reactions generated large amounts of C-S-H gel, as well as stable five-membered ring structures of mordenite and ettringite, which filled the pores and connected the soil particles. As a result, the connectivity between the pores decreased and the number of pores on the outer surfaces were significantly reduced. In addition, the height differences of the cross-sectional gullies were reduced and the surface areas were flatter, with the internal microstructures becoming more uniform and compact. This had effectively reduced the damage degrees of the Pisha-sandstone cement.

In the present study, based on the damage process of the Pisha-sandstone cement soil, a damage evolution model was established. Then, by analyzing the values of damage variable D during the initial damage stages, damage evolution development stages, and residual damage stages, it could be seen that the values of damage variable D of the modified Pisha-sandstone cement soil displayed decreasing trends with the increases in the fly ash content. Therefore, it was concluded that the incorporation of fly ash can effectively inhibit the damage process of Pisha-sandstone cement soil.

It was determined in this study that when the fly ash content levels were 6%, 9%, 12%, and 15%, the unconfined compressive strengths of the 7-day curing age were 2.17 MPa, 3.08 MPa, 3.62 MPa, and 3.63 MPa, respectively. Therefore, in accordance with the “Code for Design of Highway Asphalt Pavement” (JTG D50-2017), the additions of 6% and 9% fly ash content could be applied to the structural layers of secondary and lower secondary road pavement, and the additions of 12% and 15% fly ash content could satisfactorily meet the strength design requirements of highway and primary highway road base constructions.

In summary, this study found that Pisha-sandstone cement soil modified with fly ash was able to achieve the effective usage of large amounts of loose Pisha-sandstone and industrial waste fly ash in actual projects, which not only has high economic value but also provides new ideas for the ecological and environmental protection of the Pisha-sandstone area.

Acknowledgement: This study was supported by National Natural Science Foundation of China. The authors gratefully thank for its assistance.

Funding Statement: This study was funded by the National Natural Science Foundation of China (Grant No. 51869022).

Conflicts of Interest: The authors declare that they have no conflicts of interest to report regarding the present study.

References

1. Li, X. L., Zhai, T., Zhang, Q. (2015). Experiment on mechanical properties of Pisha-sandstone at recurrent shear. *Transactions of the Chinese Society of Agricultural Engineering*, 31(21), 154–159. DOI 10.11975/j.issn.1002-6819.2015.21.020.
2. Wu, S. Y., Li, X. L., Chang, P., Zhang, Y., Guo, L. M. (2019). Experimental study on mechanical properties of red Pisha-Sandstone Cement Soil under wetting-drying cycles. *Journal of Drainage and Irrigation Machinery Engineering*, 37(12), 1093–1099. DOI 10.3969/j.issn.1674-8530.18.0126.
3. Geng, K. Q., Li, X. L. (2020). Experimental study on mechanical properties of red Pisha-sandstone cement soil under freeze-thaw cycles. *Journal of Drainage and Irrigation Machinery Engineering*, 1–8. <http://kns.cnki.net/kcms/detail/32.1814.TH.20191204.1433.003.htm>. (In Press).
4. Tkaczewska, E. (2013). Mechanical properties of cement mortar containing fine-grained fraction of fly ashes. *Open Journal of Civil Engineering*, 3(2), 54–68. DOI 10.4236/ojce.2013.32A007.

5. Karpisz, I., Jaworski, K. (2018). Study of compressive strength evolution in soil cement samples with fly-ash admixtures. *IOP Conference Series: Materials Science and Engineering*, 365(3), 032049. DOI 10.1088/1757-899X/365/3/032049.
6. Jalal, M., Pouladkhan, A., Harandi, O. F., Jafari, D. (2015). Comparative study on effects of Class F fly ash, nano silica and silica fume on properties of high performance self compacting concrete. *Construction and Building Materials*, 94(3), 90–104. DOI 10.1016/j.conbuildmat.2015.07.001.
7. Han, X., Yang, J. B., Feng, J. J., Zhou, C. L., Wang, X. Y. (2019). Research on hydration mechanism of ultrafine fly ash and cement composite. *Construction and Building Materials*, 227(6), 116697. DOI 10.1016/j.conbuildmat.2019.116697.
8. Siddique, R. (2011). Properties of self-compacting concrete containing class F fly ash. *Materials & Design*, 32(3), 1501–1507. DOI 10.1016/j.matdes.2010.08.043.
9. Jia, L., Li, C. X., Guo, J. (2020). Mechanical properties of lime-fly ash-sulphate aluminum cement stabilized loess. *Journal of Renewable Materials*, 8(10), 1357–1373. DOI 10.32604/jrm.2020.012136.
10. Wang, D. X., Zentar, R., Abriak, N. E. (2018). Durability and swelling of solidified/stabilized dredged marine soils with class-F fly ash, cement, and lime. *Journal of Materials in Civil Engineering*, 30(3), 04018013. DOI 10.1061/(ASCE)MT.1943-5533.0002187.
11. Mohanty, S., Roy, N., Singh, S. P., Sihag, P. (2019). Estimating the strength of stabilized dispersive soil with cement clinker and fly ash. *Geotechnical and Geological Engineering*, 37(4), 2915–2926. DOI 10.1007/s10706-019-00808-1.
12. Yilmaz, Y., Coban, H. S., Cetin, B., Edil, T. B. (2019). Use of standard and off-spec fly ashes for soil stabilization. *Journal of Materials in Civil Engineering*, 31(2), 04018390. DOI 10.1061/(ASCE)MT.1943-5533.0002599.
13. Hauashdh, A., Radin, M., Radin, M. S., Jailani, J., Abd, R. J. (2020). Stabilization of peat soil using fly ash, bottom ash and portland cement: soil improvement and coal ash waste reduction approach. *IOP Conference Series: Earth and Environmental Science*, 498, 012011. DOI 10.1088/1755-1315/498/1/012011.
14. Dong, Y. P., Zhang, Y. P., Liu, Y. X. (2019). Early mechanical properties of high calcium fly ash cement soil. *IOP Conference Series: Materials Science and Engineering*, 304(2), 022040. DOI 10.1088/1755-1315/304/2/022040.
15. Yoobanpot, N., Jamsawang, P., Simarat, P., Jongpradist, P., Likitlersuang, S. (2020). Sustainable reuse of dredged sediments as pavement materials by cement and fly ash stabilization. *Journal of Soils and Sediments*, 20(10), 3807–3823. DOI 10.1007/s11368-020-02635-x.
16. Wen, H., Suo, C., Hao, Y., Fan, P., Dong, X. (2020). Effect of freezing-thawing cycle on the mechanical properties and micromechanism of red mud-calcium-based composite cemented soil. *Advances in Civil Engineering*, 2020(4), 1–14. DOI 10.1155/2020/8825576.
17. Feng, W. L., Qiao, C. S., Niu, S. J., Yang, Z., Wang, T. (2020). An improved nonlinear damage model of rocks considering initial damage and damage evolution. *International Journal of Damage Mechanics*, 29(7), 1117–1137. DOI 10.1177/1056789520909531.
18. Hu, M., Liu, Y. X., Song, L. B., Zhang, Y. (2018). Constitutive model and damage evolution of mudstone under the action of dry-wet cycles. *Advances in Civil Engineering*, (5), 1–10. DOI 10.1155/2018/9787429.
19. Zhang, Z. Y., Oeser, M. (2020). Residual strength model and cumulative damage characterization of asphalt mixture subjected to repeated loading. *International Journal of Fatigue*, 135, 105534. DOI 10.1016/j.ijfatigue.2020.105534.
20. Qu, D. X., Li, D. K., Li, X. P., Luo, Y., Xu, K. (2018). Damage evolution mechanism and constitutive model of freeze-thaw yellow sandstone in acidic environment. *Cold Regions Science and Technology*, 155, 174–183. DOI 10.1016/j.coldregions.2018.07.012.
21. Li, X. P., Qu, D. X., Luo, Y., Ma, R. Q., Xu, K. et al. (2019). Damage evolution model of sandstone under coupled chemical solution and freeze-thaw process. *Cold Regions Science and Technology*, 162(11), 88–95. DOI 10.1016/j.coldregions.2019.03.012.
22. He, R., Chen, S. F., Cong, P. L., Ji, S. H. (2013). Damage evolution model of strain hardening cementitious composites under the uniaxial stress state. *International Journal of Minerals, Metallurgy, and Materials*, 20(2), 196–204. DOI 10.1007/s12613-013-0713-8.

23. Wu, D., Zhao, R. K., Hou, W. T., Wang, S. (2020). A coupled thermo-mechanical damage modeling application of cemented coal gangue-fly ash backfill under uniaxial compression. *Arabian Journal for Science and Engineering*, 45(5), 3469–3478. DOI 10.1007/s13369-019-04118-9.
24. Zhang, J., Wang, Y. D., Su, Y. T. (2019). Fatigue damage evolution model of asphalt mixture considering influence of loading frequency. *Construction and Building Materials*, 218(4), 712–720. DOI 10.1016/j.conbuildmat.2019.05.029.
25. Rivera, J. F., Gutiérrez, R. M. D., Ramirez-Benavides, S., Orobio, A. (2020). Compressed and stabilized soil blocks with fly ash-based alkali-activated cements. *Construction and Building Materials*, 264, 120285. DOI 10.1016/j.conbuildmat.2020.120285.
26. Chen, R. F., Cai, G. J., Dong, X. Q., Mi, D. Y., Puppala, A. J. et al. (2019). Mechanical properties and micro-mechanism of loess roadbed filling using by-product red mud as a partial alternative. *Construction and Building Materials*, 216(2), 188–201. DOI 10.1016/j.conbuildmat.2019.04.254.
27. Meier, W., Kristallogr, Z. (1961). The crystal structure of mordenite (ptilolite). *Zeitschrift für Kristallographie-Crystalline Materials*, 115(1–6), 439–450. DOI 10.1524/zkri.1961.115.16.439.
28. Xu, Y., Shen, X. F., Peng, C., Ma, Y., Han, L. et al. (2018). Synthesis of ultra-small mordenite zeolite nanoparticles. *Science China Materials*, 61(9), 1185–1190. DOI 10.1007/s40843-018-9257-3.
29. Osio-Norgaard, J., Srubar III, W. V. (2019). Zeolite adsorption of chloride from a synthetic alkali-activated cement pore solution. *Materials*, 12(12), 2019. DOI 10.3390/ma12122019.
30. Fallah, M., Sohrabnezhad, S. (2019). Study of synthesis of mordenite zeolite/MIL-101 (Cr) metal-organic framework compounds with various methods as bi-functional adsorbent. *Advanced Powder Technology*, 30(2), 336–346. DOI 10.1016/j.apt.2018.11.011.
31. Chen, S. L., Ning, B. K., Bao, W. B., Jin, S. J. (2007). A damage constitutive model of cemented soil on meso-fracture process testing. *Rock and Soil Mechanics*, (1), 93–96. (In. DOI 10.16285/j.rsm.2007.01.018.
32. Ji, M., Zhang, Y. D. (2014). Damage evolution law based on acoustic emission and Weibull distribution of granite under uniaxial stress. *Acta Geodynamica et Geomaterialia*, 175(3), 269–277. DOI 10.13168/AGG.2014.0006.
33. Zhang, G. L., Jia, H. P., Wu, S. F. (2019). Study on dynamic mechanical properties and damage evolution model of siltstone. *Shock and Vibration*, 2019(3), 1–10. DOI 10.1155/2019/5174579.
34. Liu, W. B., Zhang, S. G., Sun, B. Y. (2019). Energy evolution of rock under different stress paths and establishment of a statistical damage model. *KSCE Journal of Civil Engineering*, 23(10), 4274–4287. DOI 10.1007/s12205-019-0590-4.
35. Shen, P. W., Tang, H. M., Wang, D. J., Ning, Y. B., Zhang, Y. Q. et al. (2020). A statistical damage constitutive model based on unified strength theory for embankment rocks. *Marine Georesources & Geotechnology*, 32(7), 818–829. DOI 10.1080/1064119X.2019.1633571.
36. Hui, X., Ma, F. S., Xu, J. M., Guo, J. (2017). Study on statistical damage constitutive model for rocks considering length and occurrence distribution of joint fissures. *Chinese Journal of Rock Mechanics and Engineering*, 36(S1), 3233–3238. In. DOI 10.13722/j.cnki.jrme.2016.0259.
37. Lin, Y., Zhou, K. P., Gao, F., Li, J. L. (2019). Damage evolution behavior and constitutive model of sandstone subjected to chemical corrosion. *Bulletin of Engineering Geology and the Environment*, 78(8), 5991–6002. DOI 10.1007/s10064-019-01500-7.
38. Wang, X. J., Chen, M. X., Chang, X. L., Zhou, W., Yuan, Z. H. (2009). Studies of application of Drucker-Prager yield criteria to stability analysis. *Rock and Soil Mechanics*, 30(12), 3733–3738. DOI 10.16285/j.rsm.2009.12.037.
39. Lemaitre, J., Sermage, J. P., Desmorat, R. (1999). A Two scale damage concept applied to fatigue. *International Journal of Fracture*, 97(1/4), 67–81. DOI 10.1023/A:1018641414428.
40. Xu, X. L., Karakus, M. (2018). A coupled thermo-mechanical damage model for granite. *International Journal of Rock Mechanics and Mining Sciences*, 103(11), 195–204. DOI 10.1016/j.ijrmms.2018.01.030.
41. Lemaitre, J. (1992). *A course on damage mechanics*. Berlin Heidelberg: Springer-Verlag.
42. Zhang, H. J., Zhang, X. H., Zhou, H. B. (2020). Research on acoustic emission characteristics and constitutive model of rock damage evolution with different sizes. *Advances in Civil Engineering*, 2020(16), 1–8. DOI 10.1155/2020/6660595.

43. Moran, D. A., Pantelides, C. P. (2012). Elliptical and circular FRP-confined concrete sections: a Mohr-Coulomb analytical model. *International Journal of Solids and Structures*, 49(6), 881–898. DOI 10.1016/j.ijsolstr.2011.12.012.
44. Fu, T. T., Zhu, Z. W., Cao, C. X. (2020). Dynamic behavior and damage-evolution model of frozen soil. *Meccanica*, 55(1), 177–191. DOI 10.1007/s11012-019-01100-5.
45. Zhang, Y. L., Zhao, G. F., Li, Q. (2020). Acoustic emission uncovers thermal damage evolution of rock. *International Journal of Rock Mechanics and Mining Sciences*, 132(B8), 104388. DOI 10.1016/j.ijrmms.2020.104388.
46. Hu, J. H., Yang, D. J. (2020). Meso-damage evolution and mechanical characteristics of low-porosity sedimentary rocks under uniaxial compression. *Transactions of Nonferrous Metals Society of China*, 30(4), 1071–1077. DOI 10.1016/S1003-6326(20)65278-5.